Contract No:

This document was prepared in conjunction with work accomplished under Contract No. DE-AC09-08SR22470 with the U.S. Department of Energy.

Disclaimer:

This work was prepared under an agreement with and funded by the U.S. Government. Neither the U. S. Government or its employees, nor any of its contractors, subcontractors or their employees, makes any express or implied: 1. warranty or assumes any legal liability for the accuracy, completeness, or for the use or results of such use of any information, product, or process disclosed; or 2. representation that such use or results of such use would not infringe privately owned rights; or 3. endorsement or recommendation of any specifically identified commercial product, process, or service. Any views and opinions of authors expressed in this work do not necessarily state or reflect those of the United States Government, or its contractors, or subcontractors.

Safety Analysis for Radioactive Material Processing Facility

Si Young Lee
Computational and Statistical Science Dir.
Savannah River National Laboratory
Aiken, SC 29808
Tel: (803) 725-8462
Fax: (803) 725-0141
Email: si.lee@srnl.doe.gov

Abstract – Local transient hydrogen concentrations were evaluated inside a large process room when the hydrogen gas was released by three postulated accident scenarios associated with the process tank leakage and fire leading to a loss of gas confinement. The three cases considered in this work were fire in a room, loss of confinement from a process tank, and loss of confinement coupled with fire event. Based on these accident scenarios in a large and unventilated process room, the modeling calculations of the hydrogen migration were performed to estimate local transient concentrations of hydrogen due to the sudden leakage and release from a glovebox system associated with the process tank. The modeling domain represented the major features of the process room including the principal release or leakage source of gas storage system.

The model was benchmarked against the literature results for key phenomena such as natural convection, turbulent behavior, gas mixing due to jet entrainment, and radiation cooling because these phenomena are closely related to the gas driving mechanisms within a large air space of the process room. The modeling results showed that at the corner of the process room, the gas concentrations migrated by the Case 2 and Case 3 scenarios reached the set-point value of high activity alarm in about 13 seconds, while the Case 1 scenario takes about 90 seconds to reach the concentration. The modeling results were used to estimate transient radioactive gas migrations in an enclosed process room installed with high activity alarm monitor when the postulated leakage scenarios are initiated without room ventilation.

I. INTRODUCTION

Radioactive material processing facilities such as glovebox system at the Savannah River Site are monitored for radioactive hydrogen isotope gas released into the process room. At selected threshold values, typically 4 x 10^{-5} μCi/cc, a visual and audible alarm sounds to alert workers to leave the room. The configuration of the process rooms vary significantly (room height, room width, number of sample points, response times of alarms, etc.) [1]. The purpose of this study is to demonstrate that under conservative accident scenarios with conservative initial conditions, a single sample point will result in an alarm of the radioactive gas monitoring system.

For bounding room geometry as shown in Fig. 1, high ceilings will be used as sample points are located at approximately 80 inches from the floor. The radioactive hydrogen gas source term modeled will be in the middle of the room as this is representative of most glovebox and process hood configurations. The sample point location will be 80 inches from the floor at the maximum distance from the source term (room corner). The room is considered stagnant (no ventilation) for the present work.

In this work, three releases cases will be evaluated to address tritium migration for a room fire resulting in a tank release of a small quantity of radioactive gas such as tritium, a loss of confinement from a hypothetical tank breach, and an internal tank deflagration resulting in a hot gas plume release. These three cases will be assumed to quantify the tritium migration into an unventilated room as consequence of the accidents.

- Case 1: Fire in a room leading to the breaches of a glovebox and its associated process tanks - releasing about 1 gm tritium in oxide form due to hot gas buoyancy.
- Case 2: Loss of confinement from a process tank – releasing tritium gas due to depressurization of the process tank.
- Case 3: Fire flame propagation due to the leaks of flammable mixture from the process tanks in glovebox – releasing hydrogen gas due to depressurization and hot gas buoyancy.

Based on these postulated accident scenarios in a large and unventilated process room, the modeling calculations of the tritium migration are performed to estimate local gas concentrations due to the sudden leakage and release from a glovebox system associated with the process tank.

The rate of radioactive hydrogen gas evolution released by the inadvertent opening of valve or rupturing of the pipe connected to the process tank was used in the calculations. The air circulation effect caused by the room ventilation system or leakage-in airflow was neglected here. The transient calculations were performed to evaluate local concentrations of tritium gas in the process room resulting from the sudden release of radioactive gas such as tritium during the hypothetical accident scenarios. The geometrical configurations for the air space with internal gas release near the process tank in a large process room are shown in Fig. 1.

The primary objective of the present work is to perform a modeling analysis for radioactive gas release and migration under several postulated accident scenarios without room ventilation. The modeling work was performed by taking a computational fluid dynamics (CFD) approach from the previous work [2]. A CFD model was developed to evaluate gas circulation patterns following the gas release under several postulated scenarios of tritium leakage accidents and to estimate local concentration of tritium inside a process room with 500 m^3 capacity. The modeling domain represents the major features of the process room and includes the principal release or leakage source of gas storage system as shown in Figs. 1 to 3. As shown in the figures, the computational domains for the three cases considered here were defined for the potential accident scenarios.

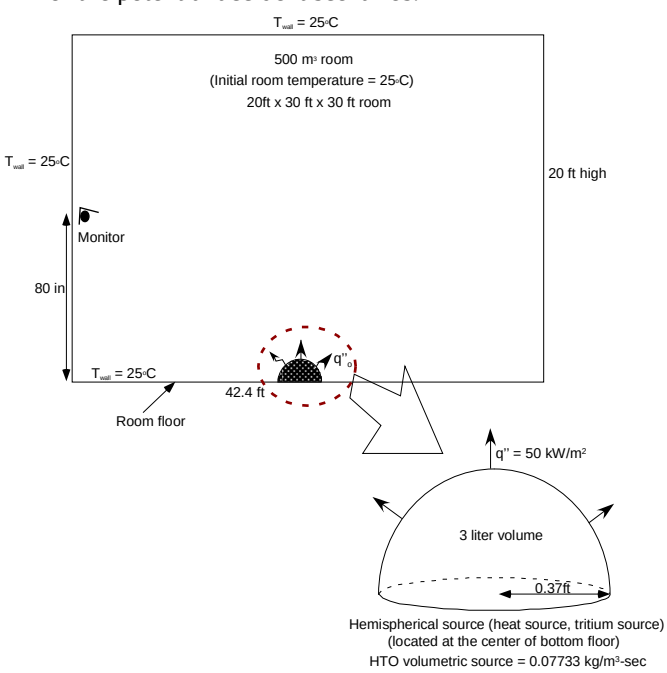

Fig. 1. Modeling domain of 30ft x 30ft x 20ft room with a heat source for the Case 1 calculations

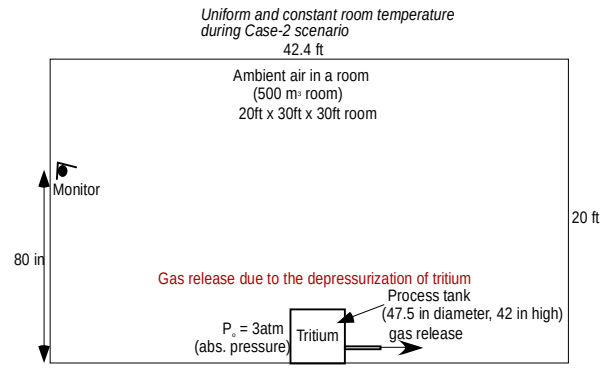

Fig. 2. Modeling domain used for the Case 2 calculations

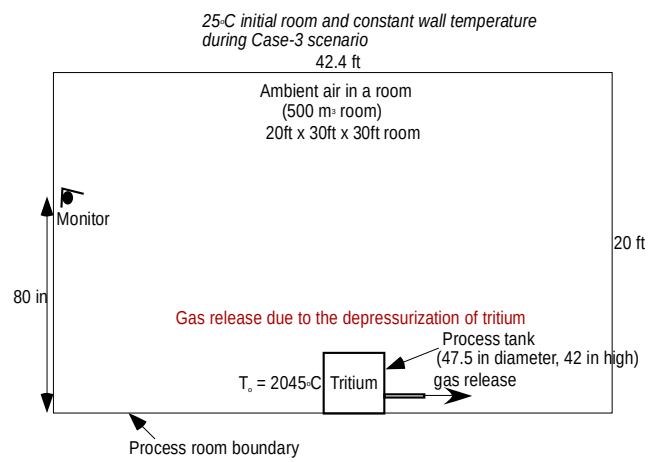

Fig. 3. Modeling domain and geometry used for the Case 3 calculations

II. SOLUTION METHOD AND APPROACH

A three-dimensional CFD approach was used to calculate flow patterns and gas release rate for the basic three cases during the accident scenarios and to compare the results for the three cases in terms of gas concentration. A finite volume CFD approach was used here to perform the gas modeling and analysis under three-dimensional prototypic domain. A prototypic geometry was modeled with a non-uniform, non-orthogonal, hybrid mesh by using FLUENT [4].

A standard two-equation, k-ε model, was used to estimate the gas turbulence. The tritium source in the process room was modeled as a momentum source. Thus, the governing equations to be solved are composed of one mass balance, three momentum equations for the three-dimensional space, two turbulence equations, and one species transport equation for tritium gas. Gas migration

inside the process room was modeled as species mixture in the governing equations.

When a tracer species, such as hydrogen, is added to the room during operations, the added species is dispersed over the room domain by natural convection. The modeling calculations for the mixing time require the balance equation of tracer species. The species balance equation is given by

$$\frac{\partial \rho Y_v}{\partial t} + \nabla \cdot \left(\rho \bar{v} Y_v\right) = -\nabla \cdot \bar{J}_v + S_v \qquad (1)$$

Y_v is local mass fraction of tracer species in the continuous fluid. $\bar{J}_v$ is diffusion flux of tracer species. S_v in the equation is a source term of tracer species added to the room air due to the release of the gas species from the source region. The diffusion flux of tracer under turbulent flow is computed by

$$\bar{J}_v = -\left(\rho D_v + \frac{\mu_t}{Sc_t}\right)\nabla Y_v \qquad (2)$$

D_v is molecular diffusion coefficient of tracer in the continuous fluid medium. Typical molecular diffusion coefficient of hydrogen species in the air is about 4.1 x 10^{-5} (m^2/sec), which is much higher than liquid species.

The computational domain boundary used for the present calculations is shown in Figs. 1 to 3.

Modeling assumptions for the calculations are as follows:

- There are no flow obstructions except for gas source region in a process room.
- Air and gas species are assumed to follow the ideal gas behavior.
- Gas release spot is located at the center of the room floor.
- Radioactive hydrogen gas evolution rate from the release spot is constant and uniform.
- There is no air ventilation in the process room.
- Air leakage into the process room is negligible.
- Room wall temperature is constant, so cooling effect through the room boundary can be ignored because of a large room.
- No chemical reactions during the gas transport and mixing process.
- Hydrogen gas is a dilute mixture component, so the mass diffusion coefficient is independent of gas composition.
- For the calculations, 4 x 10^{-5} μCi/cc gas concentration is used as the target criterion.

Hydrogen gas mass fractions for the modeling cases are computed under transient simulation conditions. The baseline conditions and modeling cases considered here are summarized in Table 1 and Table 2. All of the cases used a second order differencing scheme in order to minimize the numerical diffusion caused by the discretization. The flow conditions for the vapor space are assumed to be fully turbulent since Reynolds numbers for the nominal conditions are in the range of 10,000 based on the inlet conditions of the release spot. A standard two-equation turbulence model, the $k-\varepsilon$ model [5], was used since previous work [1] showed that the two-equation model predicts the flow evolution of turbulent flow in a large stagnant fluid domain with reasonable accuracy. A full three-dimensional representation of the entire room space was used to capture significant circulation phenomena related to the turbulent behavior of the gas flow [6]. Air was used to simulate the initially stagnant and 25°C gas in a process room.

Table 1. Baseline conditions used for the calculations

Parameters		Modeling input
Process room dimension	Height	20 ft
	Wide x Length	30 ft x 30 ft
Process room volume		About 500 m^3
Room ventilation condition		No ventilation
Process tank location containing hydrogen gas source		Center of the process room floor
Measurement location of radioactive hydrogen concentration in room		80-in elevation at the corner of room
Wall boundary conditions for room		25°C
Initial temperatures for source tank and room		25°C
Number of release events to be simulated for the present work		3 cases considered

The first case, Case 1, simulates total release of 1 gm tritium as result of the fire incident in a room leading to the breaches of a glovebox and its associated process tanks. For the Case 1 calculation, surface heat flux of 50 kW/m^2 is applied to the hemispherical source surface. The second case, Case 2, is the gas release into a large process room due to depressurization of initially 3 atm absolute tank pressure from double-ended break of 0.75-in pipe connected to cylindrical process tank of 47.5-in diameter and 42-in height. The last case, Case 3, models the accidental tritium release due to the release of flammable mixture from the process tank following the release durations of 1, 3, 5, 30 seconds from the process tank. Table 2 summarizes the three cases considered here.

Detailed modeling domains of the three modeling cases are presented in Figs. 1 to 3. From the mesh sensitivity studies, about 200,000 meshes for Case 1 and 350,000 meshes for the other cases, Case 2 and Case 3, were established, respectively. Computational meshes for three-dimensional domain of Case 1 are shown in Fig. 4. Detailed modeling domain and meshes applied to Case 2 and Case 3 are presented in Figs. 5 and 6. The major

material and physical properties used for the calculations are listed in Table 3.

Table 2. Material and physical properties used for the calculations

Parameters	Input data
Air density at initial room temperature	1.177 kg/m^3
Tritium molecular weight	6 kg/kg mol
Air molecular weight	29 kg/kg mol
Tritium oxide molecular weight	20 kg/kg mol
Hydrogen molecular diffusion coefficient in air	4.10 x 10^{-5} m^2/sec [3]
Hydrogen flame temperature in air	2045°C [3]
Turbulent Schmidt number*	0.7

Note:*: Ratio of turbulent viscosity to mass diffusion

III. CALCULATIONS AND RESULTS

The present models for the gas concentration calculations employed a three-dimensional CFD transient approach with two-equation turbulence model described in terms of turbulent dissipation and eddy diffusivity, referred to as k-ε model in the literature.[5] It assumed ideal gas behavior for the gas species in the modeling domain so that natural convection was included. The computational domains for the three cases considered here are shown in Figs. 1 to 3. The computational meshes corresponding to the tank modeling domains are shown in Fig. 4 and Fig. 6.

The primary result of the work was an estimate of the local radioactivity concentration under the imposed scenarios as summarized in Table 2. The models actually compute tritium mass concentrations. The gas radioactivity concentration was obtained by applying the conversion factor of 9690 Ci for 1 gm tritium. The radioactivity concentration of 9690 Ci/cc corresponds to a tritium mass concentration of 1gm/cc.

The benchmarking tests are chosen as three typical cases representing the turbulence model, natural convection cooling behavior, gas species mixing, and radiative heat transport since these phenomena are closely related to the gas driving mechanisms within a large air space of the tritium process room. The first three cases were benchmarked and documented in the previous work [2,6]. The last one is the heat transfer calculation by radiation. The detailed descriptions of the radiation model used here and the results are provided in the subsequent section.

III.A. Benchmarking Results

Benchmarking Test for Turbulence Flow Model

Turbulent air flow characteristics of a ventilated room were experimentally investigated by Nielsen et al. [7]. The geometrical arrangements used for their experiments are represented by Fig. 4. The figure also indicates the coordinate system and geometrical parameters. The air flow measurements were obtained at Reynolds numbers from 5,000 to 10,000. The current benchmarks of the CFD model against the test data used the test conditions as provided by Fig. 4.

The air ventilation problem assesses the capability of the k–ε model to address turbulent flow phenomena such as flow recirculation inside the ventilated room. In the benchmarking test, air flow patterns such as recirculation are assessed against the data for Reynolds number 7100, since the inlet air velocity drives the gas motion inside the ventilated room. The overall behaviors of the calculated velocity distributions were in good agreement with the test data.

Fig. 4 shows the test case modeled for a turbulent air into a room through a slit of 5 x 10^{-3} m and an inlet velocity of 10.371 m/sec (34 ft/sec) corresponding to a Reynolds number of 7,100. The air comes horizontally into the bounding wall of a rectangular room of length L, width W, and height H. Fig. 4 shows the geometrical dimensions for the rectangular room with H = 0.0893 m in terms of non-dimensional ratios.

A three-dimensional model was constructed by using the standard k-ε model to simulate air flow in a ventilated room. A steady state approach was taken to calculate the air flow patterns inside the room. The calculations were established with approximately 250,000 grid nodes from a series of sensitivity analyses and required about 3 hours of computing time on HP Linux platform. The modeling results are compared with the test results in Fig. 5. The benchmarking results for this case show that the calculated results agree with the test results within about 14%. The results demonstrate that the k-ε turbulence model can accurately predict the flow patterns for ventilation air flow in a room within about 14% relative error.

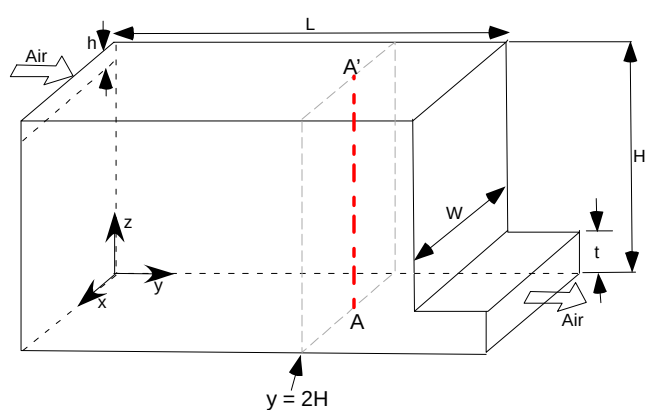

(L/H = 3.1, W/H = 4.7, h/H = 0.056, t/H = 0.16, H = 0.0893 m)

Fig. 4. Geometric arrangements and modeling coordinate system of the ventilated room used by Nielsen et al. [7]

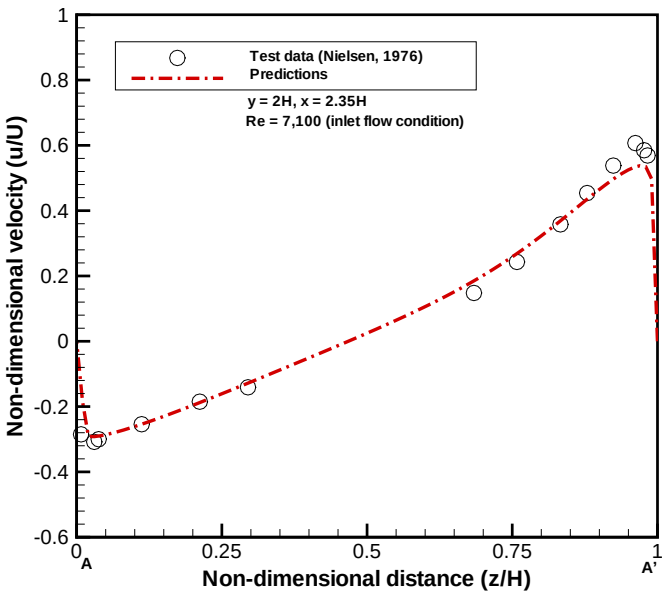

Figure 5. Comparison results of non-dimensional horizontal air velocity along the line A-A' on the plane of y=2H distance from the air inlet plane as shown in Fig. 4

Natural Convection Benchmarking Test

Primary objective of this benchmarking is to assess the modeling predictions against the analytical solutions for a natural convective flow due to the temperature gradient. A simple natural convection problem with specified boundary temperatures consists of a rectangular enclosure with adiabatic horizontal walls and isothermal vertical walls maintained at a fixed temperature difference. The temperature differences between the hot and cold walls are 10°C for the first case, Case I, and 25°C for the second case, Case II. The model calculation is based on conduction and natural convection of heat through the gas medium. The height and width of the enclosure were arbitrarily chosen to be 0.5m and 0.0254m respectively, which is an aspect ratio of about 20 and generally considered a narrow slit geometry. A schematic of this problem is shown in Fig. 6. An analytical solution for the natural convection problem can be determined for an idealized representation of the problem as fully developed flow between two infinite parallel plates as shown in Fig. 6. The momentum and energy equations for this two-dimensional problem can be expressed in the following form:

$$g\beta\left(T-T_m\right)+\left(\frac{\mu}{\rho}\right)\left(\frac{\partial^2 u}{\partial x^2}\right)=0 \qquad (3)$$

$$\left(\frac{\partial^2 T}{\partial x^2}\right)=0 \qquad (4)$$

where u is the y-direction component of the velocity and the Boussinesq approximation has been applied to the gravitational term of Eq. (3). In this case, the reference temperature for the problem is taken as arithmetic mean temperature.

For the boundary conditions

$$T=T_H \text{ at x = 0 and } T=T_L \text{ at x = L} \qquad (5)$$

The momentum and energy equations can be solved for the boundary conditions, Eq. (4) to give

$$u(x)=\left(\frac{g\beta\rho}{12\mu}\right)L^2\left(T_H-T_L\right)\left\{2\left(\frac{x}{L}\right)^3-3\left(\frac{x}{L}\right)^2+\left(\frac{x}{L}\right)\right\} \qquad (6)$$

This expression shows extrema at x/L = 0.211 and 0.789. The magnitude of the term in brackets at the extrema is ± 0.0962. This value can be multiplied by the physical constants in Eq. (6) and compared to numerical results. The physical constants used for the benchmarking test are

$$\begin{aligned} &\rho = 0.1626\ kg/m^3 \\ &\beta = 2.85x10^{-3}\ K^{-1} \\ &g = 9.81\ m/\sec^2 \qquad (7) \\ &\mu = 2.0x10^{-5}\ N\bullet\sec/m^2 \\ &L = 0.0254\ m \end{aligned}$$

With these values, the maximum velocity at the mid-plane of the rectangular enclosure is theoretically

Case I: u = 0.01176 m/sec (8)
Case II: u = 0.02939 m/sec

The profile of velocity across the width of the gap L is as important as the maximum value within the gap of the slit geometry. The modeling calculations were performed with about 10,000 mesh nodes. Table 3 also shows comparison of the peak values predicted by the model with the theoretical ones. Fig. 7 shows the profile comparison between the predictions and analytical results for Case I.

Table 3. Comparison of maximum velocities predicted by model and theory

Cases	Theory (m/sec)	Prediction (m/sec)	Relative Error (%)
Case I	0.01176	0.01129	2.84
Case II	0.02939	0.02822	2.96

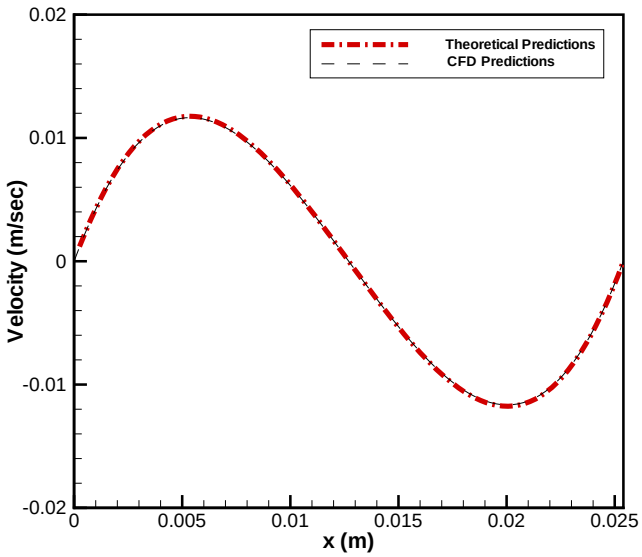

Figure 7. Comparison of the modeling predictions with theoretical results for Case I

Benchmarking Test for Gas Dispersion Behavior

The present validation work is focused on both momentum and mass diffusion under turbulent flow conditions. The literature data and information [8] clearly show that the turbulent Prandtl number (ν/α) and the Schmidt number (ν/D) are within about 10 % of 0.70, independent of the nature of the experiment and the magnitude of flow and concentration conditions. The Prandtl number is the ratio of the momentum exchange coefficient (ν) to the temperature exchange coefficient (α). Likewise, the ratio of momentum exchange coefficient (ν) to mass exchange coefficient (D) is known as the Schmidt number. The literature results show that the normalized velocity and concentration profiles are identical within the accuracy of the measurements. Therefore, the turbulent mixing calculations for this evaluation use Schmidt numbers of 0.7.

The total flow rate m at local distance x is given by

$$m = m_0 + m_1 \tag{9}$$

In Eq. (9) m_o and m_1 are gas flowrate at the inlet and total entrainment due to turbulent diffusion, respectively. The modeling predictions show that total mass flowrate increases linearly with respect to the distance x from the gas inlet from the stagnant surrounding fluid because of turbulent diffusion at the edge of the boundary layer. This is consistent with test results [10].

Figure 8 shows the modeling domain and boundary to simulate the experimental test conducted by Ricou and Spalding [10]. Detailed test conditions used for the modeling calculations are provided in Table 4. A three-dimensional turbulent steady-state approach was taken with the modeling boundary and conditions as provided by Fig. 8. The standard k-ε turbulence model was used to estimate the turbulent entrainment driven by the gas jet. The calculations were performed with about 500,000 mesh nodes. All the predictions of the six cases considered here are compared with the test results as shown in Table 4. The results show that the modeling predictions agree with the test data within about 19%.

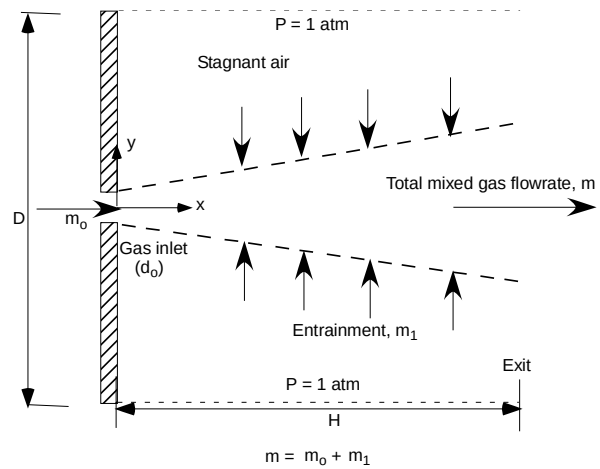

Figure 8. Test sections of Ricou and Spalding [10] as modeled for the benchmarking

Table 4. Bechmarking results of gas entrainments at exit against test data [10]

Cases	Gas injected at inlet	Reynolds number, Re*	Test data (m/m_o)	Model pred. (m/m_o)	Error (%)
Case-1	Air (air)	6.30×10^3	44.54	52.76	18.5
Case-2	Air (air)	3.73×10^4	4.46	5.26	18.0
Case-3	Air (air)	5.20×10^3	15.36	15.37	6.5
Case-4	Air (air)	3.00×10^4	8.32	9.50	14.2
Case-5	H_2 (air)	1.63×10^4	31.20	28.72	8.0
Case-6	H_2 (air)	2.10×10^4	16.70	15.17	9.2

Note: * Re = $(d_o \rho u_o/\mu)$

Benchmarking Test for Thermal Radiation

Theoretical approach for combined conduction and radiation in a non-absorbing medium such as air is taken to verify the present model under the similar physical conditions as shown in Fig. 4. The thermal and material coefficients of the package and air medium were assumed

to be independent of the temperature for the benchmarking analysis.

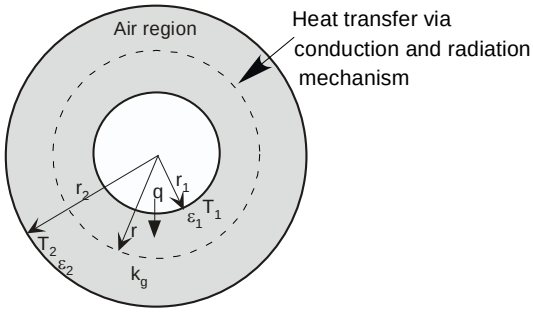

Fig. 9. Theoretical model to compute temperature distribution to include the conduction and radiation without radiative absorption.

For the regions of the annular region of the cylindrical geometry, conductive heat transfer rate per unit area through the annular air region becomes

$$q = \frac{2\pi k_s}{\ln\left(r_2/r_1\right)}\left(T_1 - T_2\right) \quad \text{for the air region } (r_1 \le r \le r_2) \qquad (10)$$

k_s in eq. (10) denotes thermal conductivities for the air region. Through the annluar region with air thermal conductivity k_g ($r_1 \le r \le r_2$), steady-state heat transfer rate per unit area (q) with radiative cooling (without convective cooling) becomes

$$q = \left(q_{cond} + q_{rad}\right)$$
$$= \frac{2\pi k_g}{\ln\left(r/r_1\right)}\left(T_1 - T_2\right) + \frac{2\pi\sigma r_1}{1/\varepsilon_1 + \left(r_1/r_2\right)\left(1/\varepsilon_2 - 1\right)}\left(T_1^{\,4} - T_2^{\,4}\right) \qquad (11)$$

q in Eqs. (10) and (11) is given by the source term at the inner wall surface. When temperature at the wall boundary line (T_1) is given by the boundary condition, temperature at the outer surface of the annular cylinder (T_2) can be computed from Eqs. (10) and (11). In this case temperature solution can be obtained by an iterative technique numerically. For the purpose of the CFD model benchmarking against the theoretically calculated results, the inner wall temperature of the cylindrically annular geometry was computed by using the numerical iteration technique when heat flux is imposed on the inner wall surface as shown in Table 5. Table 6 shows benchmarking results for the conduction-radiation coupled model in simplified annular cylinder as shown in Fig. 9.

Table 5. Modeling conditions used for the benchmarking

Physical parameters	Parameter value
Modeling geometry	Annular cylinder (Fig. 9)
Heat flux at the inner wall surface	400 W/m^2
Surface emissivities for the inner and outer surfaces (ε_1, ε_2)	0.3
Inner wall radius (r_1)	5 inches
Outer wall radius (r_2)	10 inches
Gas between the inner and outer walls	Air
Surface temperature at the outer wall	311 K (100°F)

Table 6. Benchmarking results for the conduction-radiation coupled model in simplified annular cylinder as shown in Fig. 9

Parameters	Conducted heat transfer (W/m)	Rad. heat transfer (W/m)	Inner wall surface temperature	
			^{o}C	^{o}F
Theoretical results	28.79	290.41	169.1	336.4
The modeling results	28.75	290.38	169.1	336.3

III.B. Results for the Gas Migration Models

The key transport mechanisms considered in the present work were discussed and benchmarked against the theoretical results in the previous section. The verified model was applied to the tritium process system geometry for the transient assessment of the gas flow patterns inside the air space of the process room using the boundary conditions and material properties as provided in Table 2.

The present models considered three potential cases for the estimations of the local gas concentrations within an enclosed air space. Basic modeling conditions are provided in Table 1. The modeling calculations were performed by a transient CFD method. Fig. 10 shows flow patterns driven by natural convection due to temperature gradient at 90-sec transient time during the Case 1 accident scenario. The gas is mainly raised by buoyancy effect due to heating up the room air as result of fire, and then it is spread out and retarded by the frictional resistance of the wall boundary. The red zone in the figure identifies the region in which the local velocity magnitude is higher than 1 ft/sec.

Fig. 11 shows transient temperature distributions due to heat transfer in an enclosed process room at 90 seconds since the initiation of the Case 1 scenario. As shown in Fig. 12, the results demonstrate that most quiescent air

near a solid boundary is entrained into the buoyancy-driven gas stream as the flume jet expands into the room ceiling, and then the gas flow recirculates in the room. The inner part of the flow in the vicinity of the rising flume may be expected to show a certain structural similarity to a shear-free jet, whereas entrainment of quiescent air occurs near the outer edge of the flow, which accordingly is likely to resemble a turbulent jet mixing characteristically.

When fire at a hemispherical surface without chemical reactions initially heats up a 25°C process room (30 ft wide, 30 ft long, and 20 ft high) under Case 1 scenario, the modeling results show that hot gas moves up vertically to the ceiling region of the process room and then spread out horizontally, causing the released gas to be migrated into the quiescent region of the room. Figure 13 presents transient concentrations of tritium gas along the vertical middle plane of the process room under Case 1 scenario.

The second case, Case 2, models the gas migration from the process tank into a large unventilated room due to depressurization of initially 29.4 psi gauge tank pressure from double-ended break of 0.75-in pipe connected to cylindrical process tank of 47.5-in diameter and 42-in height. Figure 14 shows transient response of average tank pressure under the pressure-driven gas movement of Case 2 scenario. The results show that mechanical equilibrium in an enclosed unventilated room is reached in about 25 seconds after the break incident. The results show that the flow patterns are very similar to those of wall jet in terms of stagnant air entrainment along the edge boundary of wall jet. When a sheared flow such as a boundary layer is forced around a turn, the slower moving gas follows a tighter radius of curvature, leading to the formation of a vortical flow, that is, secondary flow, for satisfaction of continuity. This term represents the interaction between the components of the vorticity and the velocity gradient. The results are consistent with the literature results [2].

It is noted that gas releases at high speed during the initial period of depressurization under Case 2, but gas flow is exhausted slowly after mechanical equilibrium, and it is then migrated into the other corner of the process room at transient time of 45 seconds. When gas monitor is installed at the room corner with 80-in elevation as shown in Fig. 2, transient tritium concentrations of Case 2 at the monitor are shown in Fig. 15. The calculated results show that gas concentration of 4 x 10^{-5} μCi/cc is reached at the monitor in about 13 seconds after the pipe break under Case 2 scenario. The results also show that when the monitoring point reaches the gas concentration of 4 x 10^{-5} μCi/cc, the other two corners have higher gas concentrations. It is clearly shown that transient responses of gas migration under Case 2 is much faster than that of Case 1 since pressure-driven flow of gas is faster than buoyancy-driven one.

Case 3 models the accidental gas release due to the release of flammable mixture from the process tank following the release durations of 1, 3, 5, and 30 seconds from the inadvertent opening of the valve connected to the process tank. In this case, chemical reaction is not considered as discussed earlier. When hot gas flame is released from 1-sec. valve opening and it is stopped, the results show that the gas front has traveled to the corner region of the process room opposite to the initial point of gas release in 10 seconds.

Sensitivity runs for different release durations of 1, 3, 5, and 30 seconds were made using the identical boundary and initial conditions for the assessment of the impact of gas release durations on the gas migrations into the unventilated process room under Case 3 scenario. The results clearly indicate that the gas migration is primarily controlled by the gas momentum inertia since gas diffusion due to temperature or concentration gradient is not fully evolved yet during the early transient period such as 7 seconds after the initiation of the Case 3 scenario. Thus, it is noted that the temperature and gas concentration profiles basically follow the gas flow patterns at the early transient period.

When gas monitor is located at the 80-in room corner as shown in Fig. 3, the calculated results show that gas concentration of 4 x 10^{-5} μCi/cc is reached at the monitor in about 7 seconds for 1-sec release and in about 6 seconds for the other release durations after the incident under Case 3 scenario. It is noted that the gas migration time is not sensitive to the release time as long as the gas release time is longer than 1 second. Under the same conditions, Fig. 16 compares gas concentrations between two different monitoring locations of the central and corner areas at 80 inches above the room floor. The results show that during the transient period less than 5 seconds, central area detects gas migrations more quickly than the corner area does.

The modeling results demonstrate that Case 3 scenario has the fastest response of gas migrations among the three cases considered here since it involves gas transport mechanism coupled with both processes of momentum and energy transfers. Fig. 15 shows a comparison of transient tritium concentrations at 80-in elevation of the room corner for the three cases.

It is concluded that when the alarm monitor in the process room is set as 4 x 10^{-5} μCi/cc concentration at 80-in elevation near the corner of the process room, the gas concentrations released following the postulated scenarios for Case 2 and Case 3 exceed set-point value of high activity alarm at the tritium process room in about 13 seconds, while the Case 1 scenario takes about 90 seconds to reach the triggered concentration.

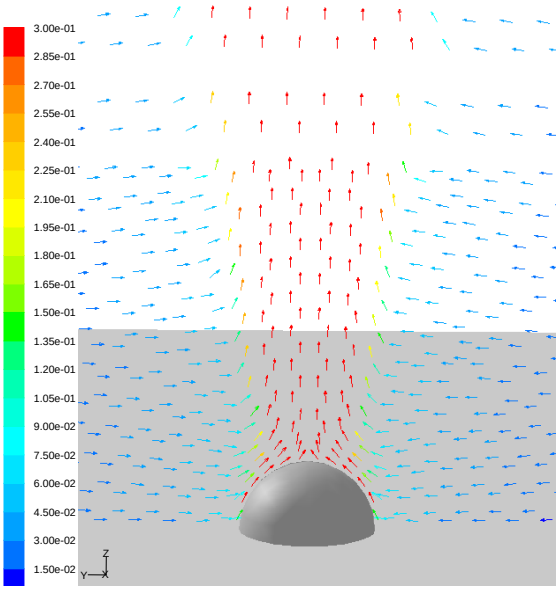

Fig. 10. Flow patterns near the room floor driven by temperature gradient at 90-sec transient time during Case 1 accident scenario (Red color code is higher than 0.3 m/sec and blue zone 0 m/sec)

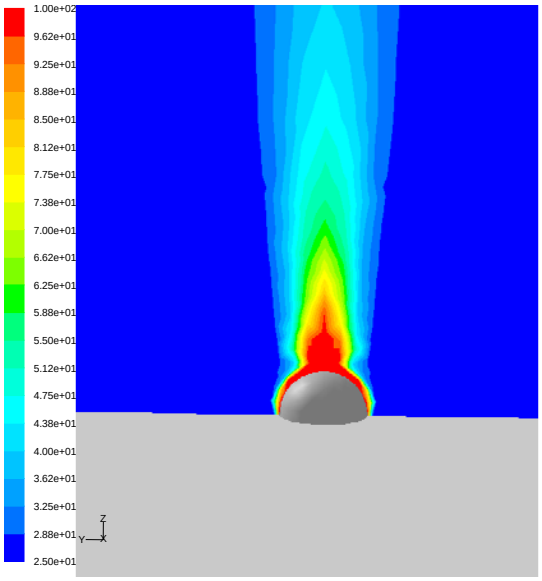

Fig. 11. Temperature distributions associated with gas migration from the hemispherical heat source on the room floor at transient time of 90 seconds under Case 1 scenario (Red zone is higher than 100°C and blue zone 25°C.)

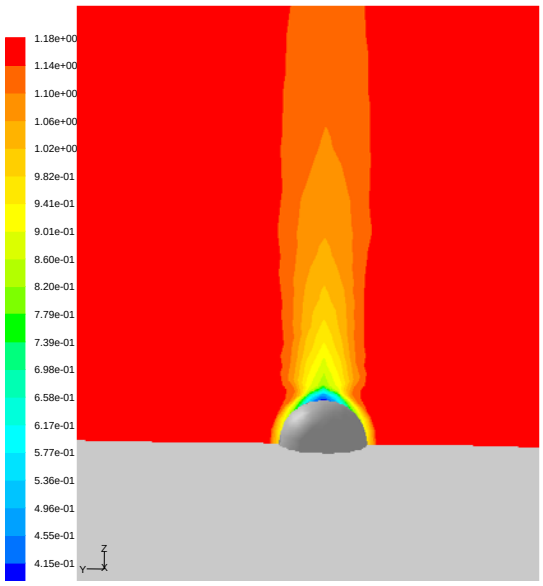

Fig. 12. Transient distributions associated with gas mixture density from the hemispherical heat source on the room floor at transient time of 90 seconds under Case 1 scenario (Red zone is 1.18 kg/m^3 and blue zone 0.37 kg/m^3.)

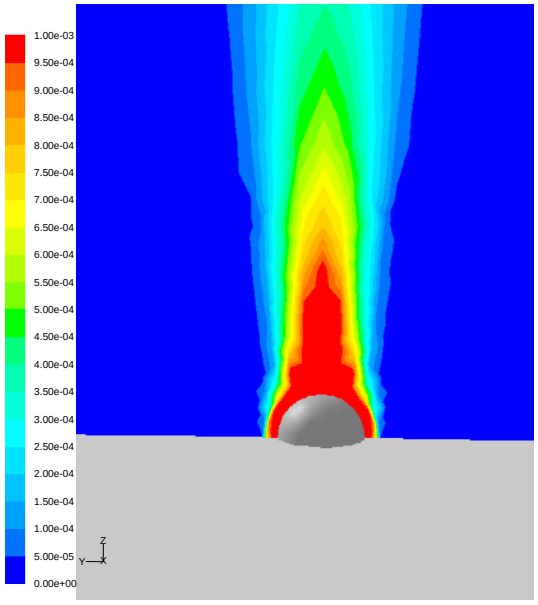

Fig. 13. Transient distributions for hydrogen gas spesies from the hemispherical heat source on the room floor at transient time of 90 seconds under Case 1 scenario (Red zone is higher than 0.001 kmol hydrogen per m^3 and blue zone is zero conc.)

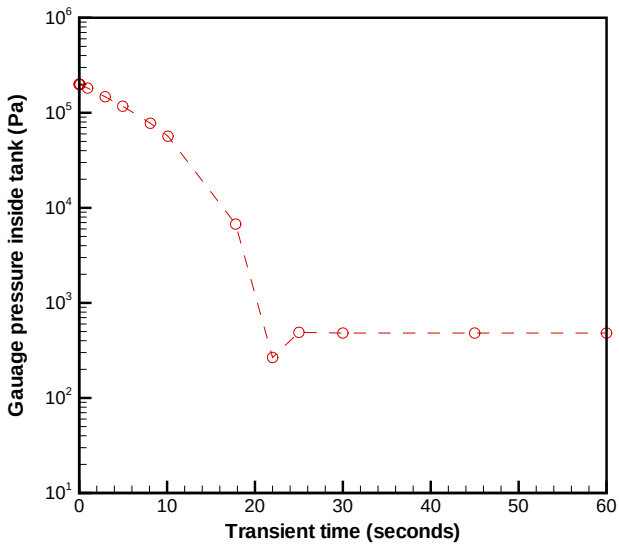

Fig. 14. Transient response to average tank pressures for the process tank under Case 2 scenario.

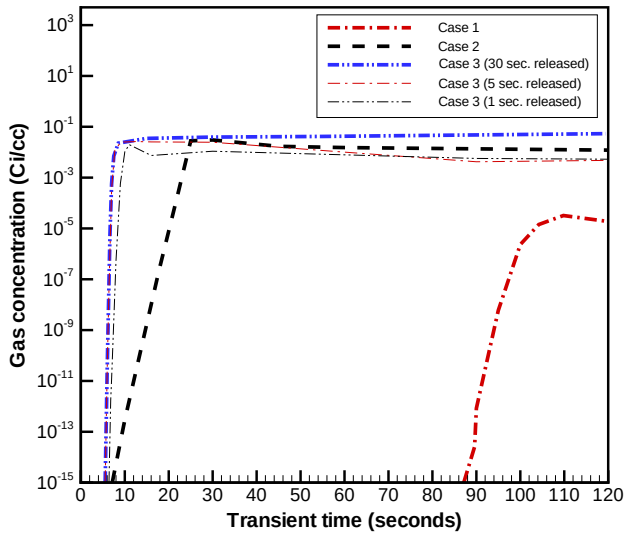

Fig. 15. Comparison of transient tritium concentrations at 80-in elevation of the room corner for the three cases.

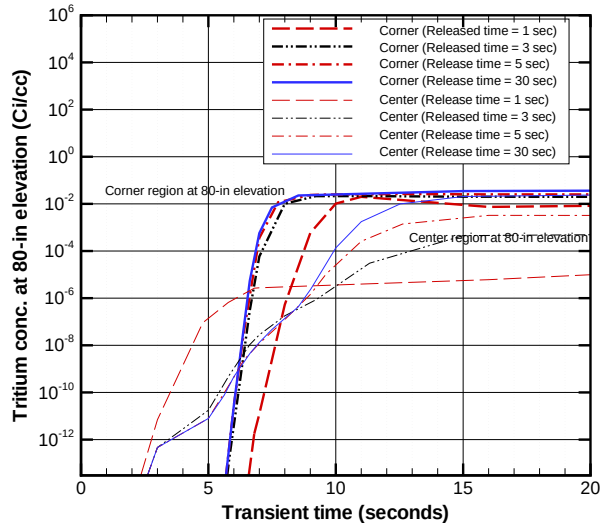

Fig. 16. Comparison of transient tritium concentrations at 80 inches above the center and corner floors of the glovebox room under Case 3 scenario.

IV. CONCLUSIONS

A transient CFD model was developed to estimate local tritium concentrations for the air space inside a large process room with glovebox system located at its floor center. The model used a three-dimensional momentum-species transport coupled approach for three postulated tritium releases due to the breach or inadvertent valve opening of a process tank. The flow conditions are assumed to be fully turbulent since Reynolds numbers for typical operating conditions are in the range of 10,000 to 70,000 based on the inlet conditions of the process component system. A standard two-equation turbulence model was used. The calculations included a gas evolution rate, buoyancy-driven natural convection effect, and forced internal circulation due to depressurization effect of the process tank. The calculations were based on prototypic geometry and three-different postulated conditions.

The modeling results showed that when the alarm in the process room was set as 4.0 x 10^{-5} μCi/cc concentration at 80-in elevation near the corner of the process room, the gas concentrations released following the postulated scenarios for Case 2 and Case 3 exceeded set-point value of high activity alarm at the tritium process room in about 13 seconds, while the Case 1 scenario took about 90 seconds to reach the triggered concentration.

ACKNOWLEDGMENTS

This work was funded by U.S. Department of Energy and performed at the Savannah River National Laboratory, which is operated by the Savannah River Nuclear Solutions, LLC.

NOMENCLATURE

atm	Atmospheric pressure
°C	Degree Centigrade (or Celsius)
Ci	Curie (3.7×10^{10} disintegration per second)
cond	Conductive heat transfer
D_v	Molecular diffusion coefficient for species
ft	foot (=0.3048m)
in	inch (=0.0254m)
$\bar{J}_v$	Diffusion flux of species
K	Absolute temperature
kg	Mass (=1000 gm)
k_g	Gas conductivity
L	Gap distance
lpm	Liter per minute
m	Meter
min	Minute
mL	Milliliter
mPa•s	MilliPascal Second
Pa	Pascal
PSD	Particle Size Distribution
q	Heat flux
r	Radius
rad	Radiative heat transfer
Sc_t	Turbulent Schmidt number
S_v	Source term in species transport equation
sec	Second
T	Temperature
W	Watt
x	Local distance along the x-axis
Y_v	Tracer mass fraction of the mixture at local point
ε	Turbulent energy dissipation rate per unit mass, or radiation emissivity
β	Volumetric coefficient of thermal expansion
ρ	Density
μ	Micro ($=10^{-6}$)
μ	Dynamic viscosity (subscript t = turbulent)
ν	Kinematic viscosity (subscript t = turbulent)
σ	Stefan-Boltzmann constant

REFERENCES

1. R. F. Farman, R. K. Fujita, and J. R. Travis, "GASFLOW Analysis of RTF, Room 9 Tritium Leak", Memorandum N-6-93-539 (K722), Los Alamos National Laboratory, June 15 (1993).
2. S. Y. Lee, R. A. Dimenna, R. A. Leishear, and D. B. Stefanko, "Analysis of Turbulent Mixing Jets in a Large Scale Tank", ASME J. of Fluids Engineering vol. 130, Number 1, pp. 011104, (2008).
3. J. H. Perry, *Chemical Engineer's Handbook*, McGraw-Hill Book Company, Inc., 3rd Edition (1950).
4. FLUENT, Ansys, Inc., Canonsburg, Pensylvania (2012).
5. W. P. Jones and P. E. Launder, "The Prediction of Laminarization with a Two-Equation Model of Turbulence", Int. Journal of Heat and Mass Transfer**, vol. 15**, pp. 301-314 (1972).
6. S. Y. Lee and R. A. Dimenna, "Applications of CFD Method to Gas Mixing Analysis in a Large-Scaled Tank", Proceedings of FEDSM2007-37366 5th ASME/JSME Fluids Engineering Conference, July (2007).
7. Nielsen, P. V., Restivo, A., and Whitelaw, J. H., "The Velocity Characteristics of Ventilated Rooms", *J. of Fluids Engineering*, Vol. 100, pp. 291-298 (1978).
8. Forstall, W., Jr. and Shapiro, A. H., "Momentum and Mass Transfer in Coaxial Gas Jets", *Journal of Applied Mechanics*, pp. 399-408, December (1950).
9. Kays, W. M. and Crawford, M. E., *Convective Heat and Mass Transfer*, Second Edition, McGraw-Hill, Inc., New York (1980).
10. Ricou, F. P. and Spalding, D. B., "Measurements of Entrainment by Axisymmetrical Turbulent Jets", *Journal of Fluid Mechanics*, Vol. 11, pp. 21-32 (1961).